Available online at www.sciencedirect.com

SciVerse ScienceDirect

Ceramics International 39 (2013) 619–627

CERAMICS INTERNATIONAL

www.elsevier.com/locate/ceramint

Wollastonite/hydroxyapatite scaffolds with improved mechanical, bioactive and biodegradable properties for bone tissue engineering

Sanosh Kunjalukkal Padmanabhan*, Francesca Gervaso, Marina Carrozzo, Francesca Scalera, Alessandro Sannino, Antonio Licciulli

Department of Engineering for Innovation, University of Salento, Lecce 73100, Italy

Received 28 May 2012; received in revised form 21 June 2012; accepted 23 June 2012
Available online 1 July 2012

Abstract

Wollastonite/hydroxyapatite composite scaffolds are proposed as bone graft. An investigation on scaffold with varying reinforcing wollastonite content fabricated by polymeric sponge replica is reported. The composition, sintering behavior, morphology, porosity and mechanical strength were characterized. All the scaffolds had a highly porous well-interconnected structure. A significant increase in mechanical strength is achieved by adding a 50% wollastonite phase. The most mechanically resistant (50/50) wollastonite/hydroxyapatite scaffolds were soaked in both simulated body fluid (SBF) and Tris–HCl solution in order to assess bioactivity and biodegradability. A carbo-hydroxyapatite layer formed on their surfaces when immersed in SBF. The biodegradability tests reveals that the composite scaffold shows a higher degradation rate compared to pure hydroxyapatite used as comparison. These results demonstrate that the incorporation of a 50% of wollastonite phase in hydroxyapatite matrix is effective in improving the strength and the bioactive and biodegradable properties of the porous scaffolds.

Keywords: A. Sintering; B. Composites; E. Biomedical applications; Calcium phosphate

1. Introduction

Tissue engineering is a useful tool for the reconstruction of massive bone defects such as diseased or damaged bone [1]. One of the promising research outcomes of tissue engineering is the development of porous bioceramic scaffolds for bone regeneration [2]. Ideal scaffolds for bone tissue regeneration require three-dimensionally interconnected porous structures to allow cell migration, vascularization and nutrient diffusion [3,4]. In order to induce optimal osteogenesis throughout the scaffolds and the surrounding tissue, 3D scaffolds need to have the appropriate physical and biological properties such as pore size, pore structure, surface topography, chemical composition, mechanical strength and degradation rate [5]. For porous bioceramics scaffolds, several production methods have been developed. These include solid freeform fabrication, polymer sponge replica, salt leaching, dual phase mixing and gel casting [6–9]. Polymeric sponge replica method has got prominent attention due to its potential of forming uniform dispersion of ceramic powder within the polymeric struts and high porosity and interconnected pores of the obtained scaffolds.

Calcium phosphate based biomaterials have been developed for hard tissue repair because of their excellent biocompatibility and osteoconductivity [10]. One of the most widely used synthetic calcium phosphate ceramics is hydroxyapatite (HA) due to its chemical similarity to the inorganic component of hard tissues [11]. Unlike other calcium phosphates, HA does not break down under

*Corresponding author. Fax.: +39 8321830130.
E-mail addresses:
sanosh2001@gmail.com (S. Kunjalukkal Padmanabhan),
francesca.gervaso@unisalento.it (F. Gervaso),
marina.carrozzo@unisalento.it (M. Carrozzo),
francesca.scalera@unisalento.it (F. Scalera),
alessandro.sannino@unisalento.it (A. Sannino),
antonio.licciulli@unisalento.it (A. Licciulli).

0272-8842/$36.00
http://dx.doi.org/10.1016/j.ceramint.2012.06.073

physiological conditions. It is thermodynamically stable and takes part actively in bone bonding, forming strong chemical bonds with the surrounding bone. However, HA scaffold with high porosity (i.e. $>90\%$) is extremely brittle; practice indicates that the use of HA without additives for load bearing bone regeneration application is inefficient due to its low strength. There have been many attempts to improve the mechanical properties of HA scaffold by fiber and whisker reinforcement, coating with bioactive glass, bioactive polymers and nano-composites [12,13]. Another approach to improve the mechanical properties of HA is to combine it with a tougher phase, producing a composite and overcoming its mechanical limitations by reinforcing it with suitable materials [14].

In recent years, calcium silicate based bioceramics have been studied as potential substitutes for hard tissue like bone, because of their superior bioactivity compared to HA [15]. This property is attributed to the presence of silicon, which plays an essential role in the metabolic events that induce a new bone formation. The wollastonite $CaSiO_3$ (WS), one of the forms of calcium silicate ceramic, has been widely used as a filler to fabricate HA composites with improved mechanical properties. The WS phase in the composite ceramic consists of a silica chain structure. The acicular nature of WS minerals allows it to compete with other fibrous materials, such as ceramic fiber, glass fiber as a reinforcement phase.

This acicular structure has been reported to reinforce also the apatite crystals [16]. Recent studies reveal that the addition of various amounts of WS in WS–HA sintered composite has an improvement on its mechanical property, bioactivity and biodegradability [17,18].

In our recent papers [19,20], we reported the fabrication of HA and WS/HA composite scaffolds using polymeric foam replica method. Aim of this study was to investigate the influence of adding a WS acicular phase in HA matrix on mechanical properties of a highly porous scaffold. We considered the WS/HA system as a composite structure in which WS and HA are reinforcement and matrix phase respectively. A detailed investigation on the dependence of both mechanical and functional properties on the WS/HA weight ratio was performed. More in detail, the effect of WS/HA ratio on the microstructure, sintering behavior and mechanical strength was assessed. Moreover, the bioactivity and biodegradability of the best performing WS/HA sample was also evaluated by in-vitro tests having the pure HA as a reference system.

2. Materials and methods

2.1. Synthesis of the HA powder

Submicronic HA powder was synthesized by precipitation technique [21]. Briefly describing $Ca(NO_3)_2 \cdot 4H_2O$ (Sigma Aldrich, Germany) and H_3PO_4 (Sigma Aldrich, Germany) were the precursor for calcium and phosphorous respectively. One litre of 0.3 M H_3PO_4 was prepared in double distilled water. To this solution, ammonia was added under stirring till a constant pH = 10 was obtained. To this solution 1 litre of 0.5 M $Ca(NO_3)_2 \cdot 4H_2O$, was slowly added maintaining a Ca/P ratio of 1.67. The solution was kept at constant pH = 10 by adding small amounts of ammonia. The solution was rigorously stirred for 1 h and kept for ageing for 24 h at room temperature. The precipitates were filtered out using Buchner funnel, washed repeatedly using double distilled water to remove NH_4^+ and NO^{3-} and dried at 65 °C for 24 h in an oven. The dried powder was calcined in air at 900 °C for 60 min using a heating rate of 5 °C/min. The calcined powder was grinded using a planetary ball mill with zirconia balls as grinding media for 30 min. After milling, the slurry was dried in air oven and sieved through 80 μm mesh to obtain the final powder for fabrication of the scaffolds. WS powder (Alfa Aesar), was selected. The composition of both prepared HA900 and commercial WS powders were analyzed by X-ray diffraction (XRD: D/max 2550V, Rigaku Co., Tokyo, Japan). The morphology of the HA powder and WS acicular reinforcement particles were observed with scanning electron microscope (SEM: Zeiss-EVO)

2.2. Forming and sintering of the porous scaffolds

Foam replication method was adopted for the production of bioceramic scaffolds. The slurries were prepared by adding different proportions of HA and WS powder in double distilled water and mixed using a magnetic stirrer. In all slurries the powder was added up to a final concentration of 70 wt% and polyvinyl alcohol (PVA) was used as binder at 2%wt. A carbonic acid based poly electrolyte (Dolapix CE-64, Zschimmer-Schwarz, Germany) was used as deflocculating agent of the ceramic suspension. The polyurethane sponges used as template (density of 30 kg/m^3, 25 ppi, kindly provided by ORSA Foam S.p.A.) were cut in cube of 1.5 cm length, impregnated with slurries, gently squeezed to remove the exceeding suspension and dried at room temperature for 24 h. The infiltrated sponges were heat treated to 500 °C at a ramp rate of 1 °C/min in order to burnout the polyurethane foam. After 1 h at 500 °C, the samples were sintered at 1300 °C for 3 h. The scaffolds produced contain 0, 25, 50, 75, and 100 wt% of WS, coded as 100HA, 25WS–75HA, 50WS–50HA, 75WS–25HA and 100WS respectively.

2.3. Morphology and composition of starting powders and sintered scaffolds

The morphology, pore shape and size of sintered scaffolds were observed with scanning electron microscope. The phase composition of the starting powders and the sintered scaffolds (25WS–75HA, 50WS–50HA, 75WS–25HA) were evaluated by X-ray diffraction. The linear shrinkage (δ) of the samples during sintering was assessed by measuring the dimensions of the sample using a calliper before and after the sintering process. Each sample was

weighed after the sintering process and the bulk density was calculated as the ratio between the weight and the volume of the specimen. The porosity of the ceramic foams was calculated using the following:

$$P = 1 - \frac{\rho}{\rho_0} \quad (1)$$

where ρ is the bulk density and ρ_0 is the apparent density of dense material, measured using picnometer (Quantachrome).

2.4. Mechanical characterization

The compressive strengths of the different scaffolds (dimensions $15 \times 10 \times 10\ mm^3$) were measured using a universal testing machine (Lloyd LR5K instrument, Fareham Hants, UK) equipped with a 1 kN load cell at a crosshead speed of 0.5 mm/min. During the compressive test, the load and displacement were monitored and recorded. Five samples from each group were tested to obtain average value of porosity, linear shrinkage and mechanical strength with their standard deviation.

2.5. Evaluation of bioactivity in SBF

The bioactivity of 50WS–50HA composite scaffold was investigated in simulated body fluid (SBF) which was prepared following Kokubo method [22] with a concentration of 1.5 M. Briefly, analytical reagent grade NaCl, $NaHCO_3$, KCl, K_2HPO_4, $MgCl_2$, $CaCl_2$, and Na_2SO_4 were dissolved in distilled water and the solution was buffered to pH 7.4 at 37 °C with tris(hydroxymethyl)aminomethane and hydrochloric acid (HCl). The samples were soaked in the SBF at 37 °C for 1, 3, 7, 14 and 28 days. Plastic containers were used for all the SBF preparations and experiments. The ratio of solution volume to scaffold surface area was equal to 0.001 mL mm^{-2}. After soaking, samples were taken out and gently rinsed with distilled water and dried at 150 °C for 48 h. The formation of bone-like HA on the surface of the samples was investigated by XRD and SEM coupled with energy-dispersive spectroscopy (EDS:Bruker). The variation of Ca, P, and Si ion contents in the SBF solution was measured using inductively coupled plasma atomic emission spectroscopy (ICP-AES) iCAP 6000 Series (Thermo Scientific). Three samples for each experimental point were analyzed.

2.6. Evaluation of degradability in Tris–HCl buffer solution

The degradability of the 50WS–50HAscaffolds was evaluated measuring the weight loss of the samples in Tris–HCl buffer solution [23]. The 0.05 M Tris–HCl buffer solution was prepared dissolving Tris(hydroxymethyl)aminomethane (analytical reagent grade) in distilled water and then was buffered to pH 7.4 at 37 °C with HCl. The samples were soaked in the Tris–HCl buffer solution for different periods (1, 3, 7, 14 and 21 days) at 37 °C with the ratio of surface area to solution volume of 0.001 mL mm^{-2}. The Tris–HCl buffer solutions were refreshed every 24 h. After various soaking periods, the samples were removed from the Tris–HCl buffer solution, gently rinsed with distilled water and dried in vacuum at 150 °C for 48 h before characterization. Three samples from each group were tested to obtain an average degradability. Moreover, also 100HA scaffold underwent the same experimental procedure as mentioned above.

3. Results

3.1. Characterization of HA and WS powders

SEM image of HA powder calcined at 900 °C is given in Fig. 1a. The powder looks agglomerated; particles average size is 150 nm and is spheroid in shape. The SEM image of WS powder (Fig. 1b) shows a large fraction made of acicular particles with length in the range 20–50 μm. The phase analysis by X-ray diffraction reveals that no phases other than WS-1A (JCPDS 84-0654) and HA (JCPDS 09-0432) are present in the respective powders (Fig. 2).

3.2. Scaffolds characterization

Fig. 3 shows the XRD patterns of the scaffold at different WS/HA weight ratio after sintering at1300 °C for 3 h. Compared with standard XRD pattern of HA and

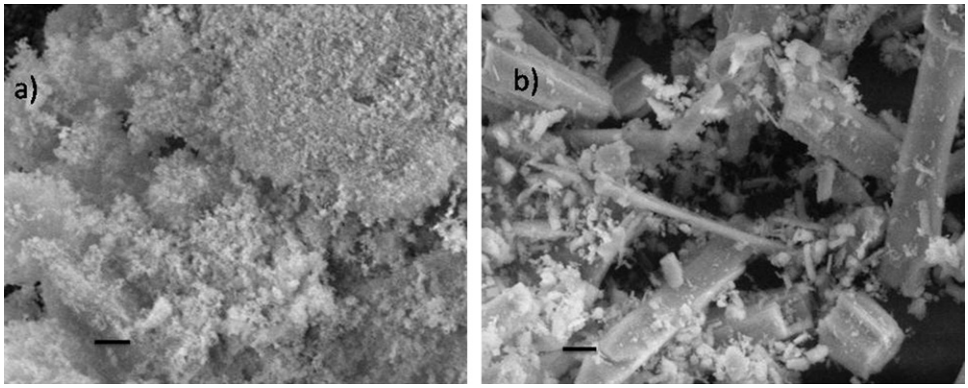

Fig. 1. SEM images of starting powders (a) HA powder calcined at 900 °C and (b) commercial WS powder (scale bar for both powders 5 μm).

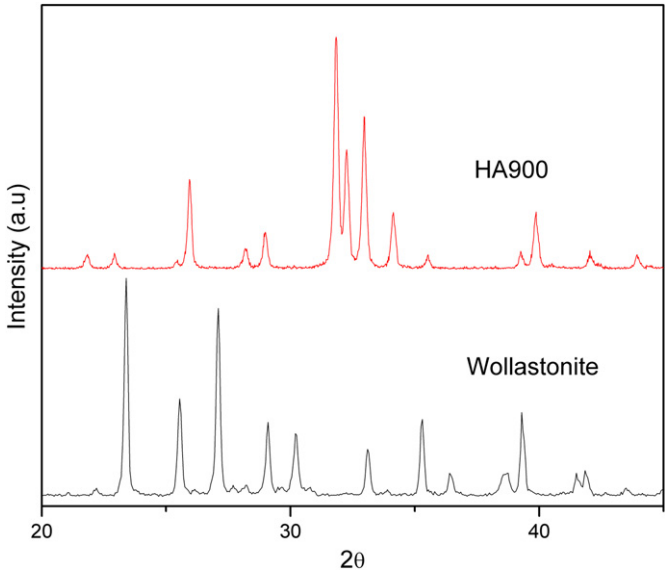

Fig. 2. XRD patterns of the starting powders. HA powder calcined at 900 °C and commercial WS powder.

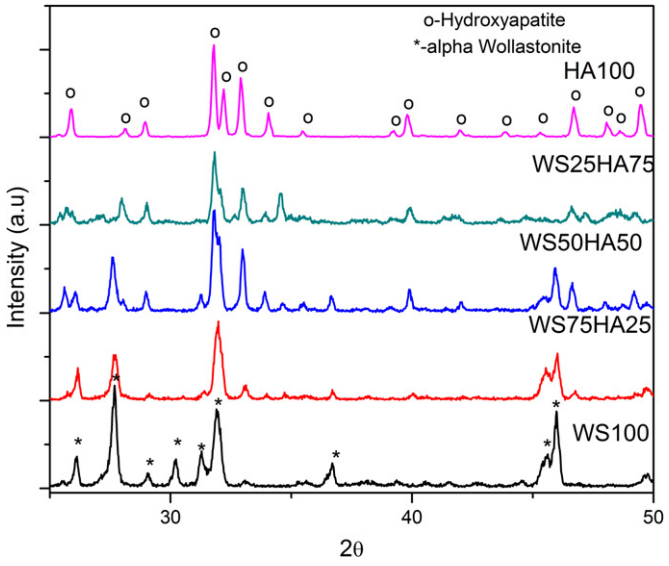

Fig. 3. XRD patterns of the composite scaffold with different weight ratio after sintering at 1300 °C for 3 h (a) 100HA, (b) 25WS–75HA, (c) 50WS–50HA, (d) 25HA–75WS and (e) 100WS.

pseudo-WS (JCPDS 74-0874), it can be seen that the scaffolds are composed of crystalline HA and WS-2M (alpha form), no other phases can be observed.

The macrostructure of the different scaffolds sintered at 1300 °C is shown in Fig. 4(a–e). All scaffolds have an open porosity and highly interconnected pores with pore size > 500 μm irrespective of the weight ratio of powders used.

SEM images shown in Fig. 4(f–j) represent the microstructure of sintered scaffolds with various WS/HA weight ratios. Fig. 4f shows the microstructure of 100HA scaffold and reveals the very good sintering ability of the spheroid HA particles, resulting in well defined grain boundaries without any defects like cracks and pores. The microstructure of all other scaffolds shows a compact microcrystalline appearance with clear grain boundaries and some micrometer size pore. Moreover, it can be observed that, fiber shaped grains are distributed in the sintered matrices and the amount of these fibers increases remarkably as the WS amount increases. In the case of 25WS–75HA scaffold, some pores result from the insufficient quantity of WS fibers within the HA matrix (Fig. 4g). Conversely the WS fibers are well embedded in the 50WS–50HA scaffold without any micropore formation (Fig. 4h).

The effect of WS/HA ratio on linear shrinkage, porosity and compressive strength of sintered samples is shown in Table 1. The 100HA scaffold have a linear shrinkage and a porosity of 19% and 91% respectively while the 100WS scaffold have a linear shrinkage 6% and a porosity 90%. The linear shrinkage of the sintered composite scaffolds changes from 17.3% to 10.6% when the WS/HA ratio increases from 1/4 to 3/4, while all the scaffolds have a porosity of about ~90% irrespectively of the weight ratio.

The 100HA scaffold without any reinforcement has a compressive strength of 0.51 MPa. With the increase of WS amount, the compressive strength initially increases and value of compressive strength equal to 0.62 and 1.02 MPa is obtained for 25WS–75HA and 50WS–50HA scaffolds respectively. However, a further increases in WS content (samples 75WS–25HA and 100WS) results in a drop of the compressive strength (0.67 and 0.21 MPa respectively).

3.3. Scaffold bioactivity

In vitro bioactivity of the most mechanically resistant 50WS–50HA scaffolds were investigated by soaking them in concentrated SBF (1.5SBF). Fig. 5a shows the SEM micrographs of 50WS–50HA scaffold after immersion in the 1.5SBF for 7 days. The surface of the scaffold appears modified suggesting that a pronounced mineralization, with the formation of new and denser apatite layers, occurred. Grain boundaries cannot be clearly distinguished anymore, little cracks appear and agglomerated particles of newly formed material can be observed on the surface of the sample. EDS spectra given in Fig. 5b reveals that the surface of the scaffold after SBF immersion for 7 days is composed of Ca and P whereas Si is not detected. Also XRD pattern shown in Fig. 6 reveals that after SBF treatment for 7 days, some WS phase peaks decreased in intensity and some completely disappeared. On the other hand, the HA peaks become more prominent compared to the HA peaks before SBF immersion.

The variation of Ca, P and Si ions for the 50WS–50HA scaffolds soaked in SBF solution were evaluated at different time intervals using ICP and the results are presented in Fig. 7. The concentration of Ca and Si in the solution increased with the increasing immersion time. On the contrary, the concentration of P ions slowly decreased in the early stages and then declined rapidly to almost zero during the period from 4 to 14 days. The rate

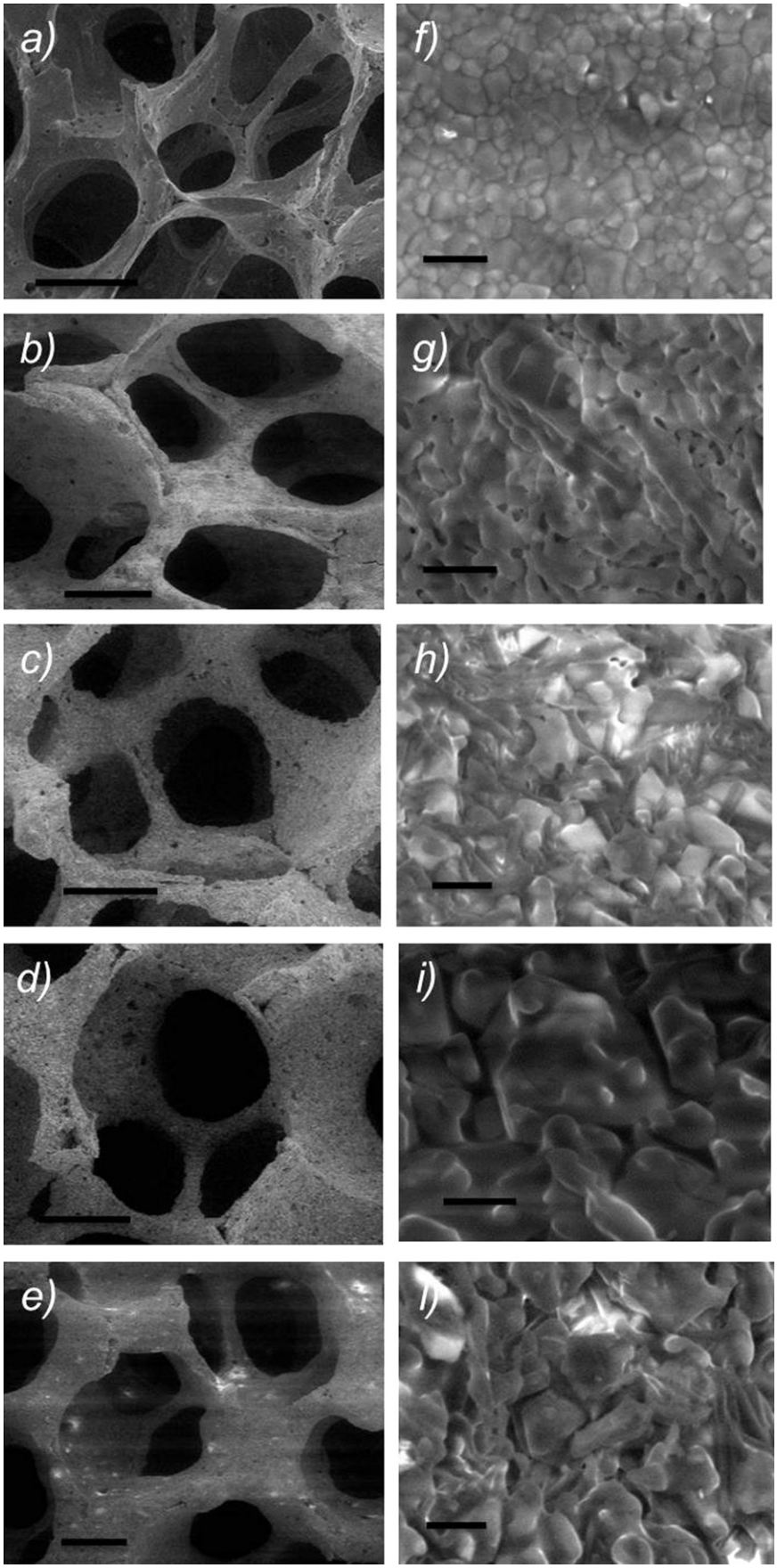

Fig. 4. SEM images of the scaffolds with different WS/HA ratios sintered at 1300 °C for 3 h. Images (a–f) macrostructure of 100HA, 25WS–75HA, 50WS–50HA, 75WS–25HA and 100WS respectively (scale bar 500 μm) and images (f–h) microstructure of respective scaffolds (scale bar 10 μm).

Table 1
Linear shrinkage, porosity and compressive strength of scaffolds sintered at 1300 °C for 3 h.

Sample ID	100HA	25WS–75HA	50WS–50HA	75WS–25HA	100WS
Linear shrinkage (%)	19 ± 3	17.3 ± 3	15.5 ± 3.1	10.6 ± 1.5	6 ± 1
Porosity (%)	91 ± 2.4	90 ± 3	89.9 ± 2	88.5 ± 1	90 ± 3
Compressive strength (MPa)	0.51 ± 0.14	0.62 ± 0.11	1.02 ± 0.16	0.67 ± 0.14	0.21 ± 0.1

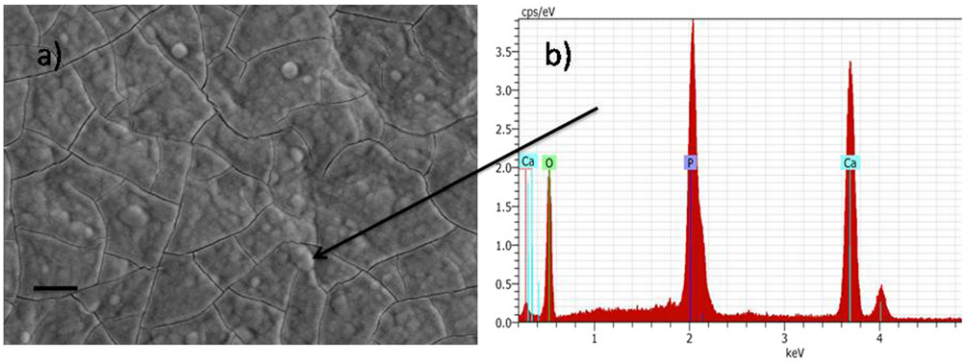

Fig. 5. (a) SEM micrograph (scale bar 20 μm) and (b) EDS spectra of the 50HA–50WS scaffold after immersion in the 1.5SBF for 7 days.

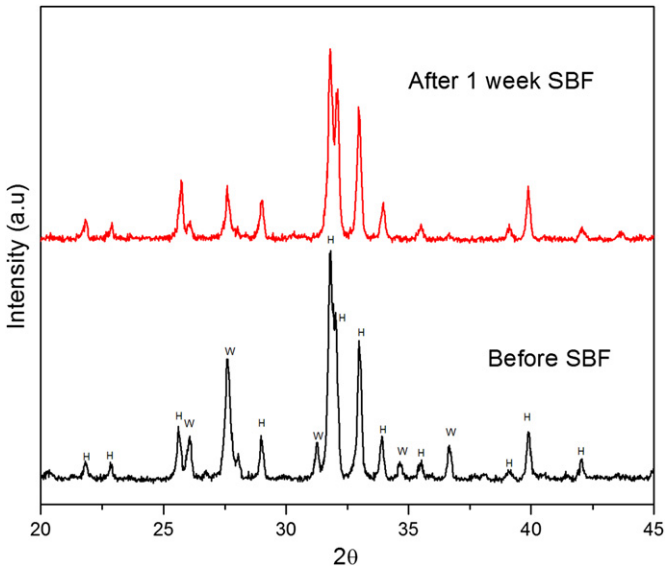

Fig. 6. XRD pattern of the 50HA–50WS scaffold before and after immersion in the 1.5SBF for 7 days.

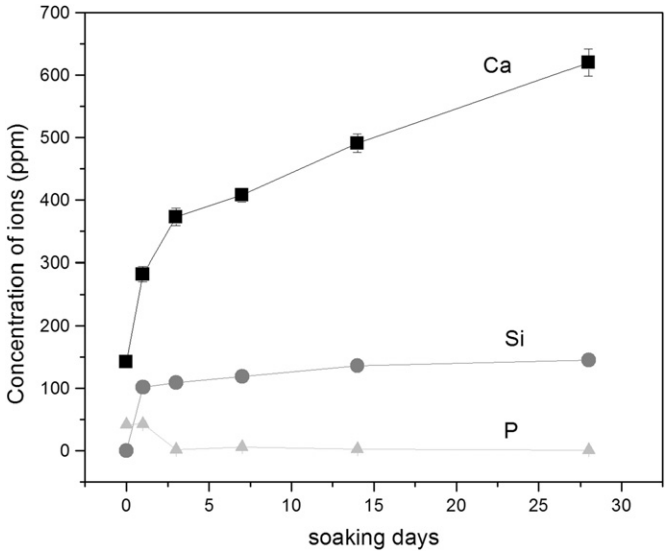

Fig. 7. Variation of Ca, P and Si ions for the 50WS–50HA scaffolds soaked in SBF solution at different time intervals using ICP.

of Ca release to the solution is higher than the rate of Si release. In fact, while the dissolution of both HA and WS phases causes Ca release, Si and P can only be released from the WS and HA phases respectively.

3.4. Scaffold biodegradability

The degradability (weight loss percentage, wt%) trend of 100HA and 50WS–50HA composite scaffold in Tris–HCl buffer solution is shown in Fig. 8. A significant difference in degradation rate was observed for both the scaffolds. After one day the degradation of pure HA scaffold reached 2.5% while on 50WS–50HA scaffold it was 7%. Degradation in terms of weight loss had an almost linear dependence on time. On day 21, the degradation rate of 50WS–50HA scaffold reached 34% showing a weight loss almost 14 times higher than the degradation rate of pure HA scaffold.

4. Discussion

WS/HA composite scaffolds with different weight ratios were properly formed by means of polymeric sponge replica method. All types of scaffolds showed high and

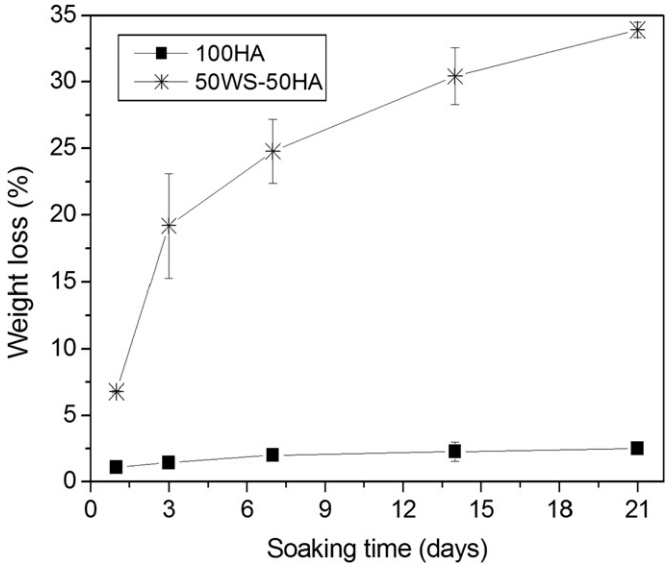

Fig. 8. Degradation rate of 50WS–50HA scaffold and 100HA scaffold versus various soaking time in Tris–HCl.

interconnected porosity that, as reported by several studies, is mandatory for scaffold osteointegration and cell proliferation [24]. Moreover, the scaffolds could be easily prepared with pore size higher than 500 μm that is higher than 300 μm, a threshold value for enhanced osteogenesis [25].

The XRD results show that the incorporation of WS into HA phase does not induce any transformation of HA into any other calcium phosphate phases or intermediate phases. It has been reported that above 1125 °C, phase transformation of beta-WS into alpha-WS occurs [26]. In the case of HA, no phase transformation occurred due to the high thermal stability of the submicron sized starting powder [19].

From morphology evaluation by SEM pictures on sintered samples it appears that the acicular shape of many WS particles is maintained even if modification occurs especially on small WS particles. Such acicular WS particles look well embedded into the HA phase (matrix) as the weight of the WS was lower than the HA matrix. Although the WS particles could be clearly distinguished within the HA matrix, the surface appeared almost homogenous and regular with the two phases in intimate contact with each other. When the weight percentage of WS was more than HA matrix, microstructure modification and grain growth occur, together with the formation of larger fraction of interstitial pores (Fig. 4i and j). This phenomenon can be attributed to the presence of a larger fraction of WS big particles with the smaller particle fraction unable to reshape and compact up to full removal of interstitial pores trapped inside the large particles.

The hypothesis of high refractoriness at increasing WS content is also coherent with the lower linear shrinkage measured when WS phase increased. We assume that the decrease in linear shrinkage is mainly due to the particle size and thermal stability of WS whose melting temperature is 1540 °C. Therefore, when the amount of WS reinforcing phase in HA matrix increases, the reinforcing WS particles do not get enough HA matrix to fill interstitial spaces. This phenomenon becomes evident when WS phase is higher than 50 wt%. Although an increase in the scaffold pore size is desirable from a biological point of view, we must remember that it has a negative impact on the mechanical property of the structure.

Mechanical properties of ceramics are strongly influenced by morphology, porosity and grain size [27,28]. In order to increase the mechanical strength of a highly porous structure, our approach was the addition of a reinforcing phase within a HA matrix. Due to its acicular form WS has found extensive applications as a reinforcing phase in polymer matrix composites, coatings, friction applications. In all this application it has been found that WS improves material strength. In our case a significant increase in the mechanical strength was obtained when WS was added in a percentage not higher than 50% to the HA matrix. The higher increase in strength was observed in the case of 50WS–50HA and is probably due to the fact that WS crystals were properly locked between HA particle (Fig. 4h). At WS percentage higher than 50%, the strength decreased because of the formation of micropores and abnormal grain growth during sintering. Wu et al. [29] reported that WS scaffolds with 81.5% porosity have a compressive strength of 0.3 MPa. The 100WS scaffolds of present study have almost same strength if we consider their higher porosity (90%). We explain the low compressive strength of 100WS scaffold with the low sintering ability of WS powder at the sintering condition used in the present study. The acicular WS particles play a dominant role in the mechanical properties of WS/HA samples. The amount of acicular particles increases remarkably with the increase of the WS amount (Fig. 3). Previous studies confirm that these interactions can be represented as system made of a short fiber reinforcing phase (WS) in a brittle matrix (HA) with reinforcing and toughening mechanisms like fiber pullout and debonding [18,30]. After certain extent, the amount of HA matrix is not enough for the WS reinforcements and it results in inefficient sintering. As a consequence, a smaller shrinkage will occur and low mechanical properties will be recorded (75WS–25HA and 100WS scaffolds, Table 1).

The compressive strength of the 50WS–50HA (porosity 90%) scaffolds prepared in this study was 1.02 MPa, significantly higher than those reported in previous studies on porous HA scaffolds and 45S5 Bioglass scaffolds (porosity 84–89%) prepared via polymer sponge template method were about 0.51 and 0.42–0.6 MPa respectively [19,30]. The compressive strength of spongy bone (not the strut) is in the range of 0.2–4 MPa, when porosity is 90% [31]. In our case the measured compressive strength of all the scaffolds irrespective of the weight ratio of composite falls in this range (Table 1) and mimics that of cancellous bone.

The in vitro tests performed by soaking the 50WS–50HA scaffolds in SBF solution demonstrated their bioactivity. The ICP results confirmed that the concentration of Si, Ca and P ions change in the SBF solution, suggesting that carbo-apatite layer formed on the composite scaffold surface. This effect is due to the fast dissolution of silica from WS in to the SBF medium and formation of apatite layer on the scaffold. More in detail, Ca ions are released to the solution, exchanging hydrogen ions to form a hydrated silica leaching layer on the WS particles surface that contains Si–OH groups, which have been proposed as a catalyzing agent for the nucleation and growth of the bone-like apatite layer. On the other hand, the dissolution of ions increases the degree of super saturation of the SBF with respect to apatite, leading to the precipitation of the apatite on the sample surfaces. As soon as apatite nuclei are formed, they grow spontaneously by consuming the calcium and phosphorus ions from the surrounding fluid [32]. The formation of the bone-like apatite from SBF has proven the bone-bonding ability of material in vitro.

One of the important characteristics that a scaffold must full fill is its degradability [33]. The present study demonstrated that the obtained 50WS–50HA scaffold exhibited weight loss in Tris–HCl solution and its dissolution rate was higher than that of 100HA scaffold over all the degradation time, which indicated that the 50WS–50HA composite scaffold were degradable. The higher dissolution rate of 50WS–50HA composite scaffold is attributed due to the presence of WS phase which remarkably dissolves when immersed in Tris–HCl [34,35].

5. Conclusions

WS/HA scaffolds were fabricated by sponge replica method using home synthesized HA powder and commercial WS acicular powder. The scaffolds could be easily sintered without significant decomposition or phase changes demonstrated by XRD analysis. All types of scaffold showed porosity around 90% and pore size more than 500 μm.The effects of the WS/HA ratio on the sintering behavior, microstructure and mechanical strength were carefully investigated. With the increase of WS component, linear shrinkage of the composite ceramics decreased, while the porosity did not show much difference. The compressive strength of the sintered samples increased from 0.51 ± 0.14 to 0.62 ± 0.11 and 1.02 ± 0.16 MPa when adding 25 and 50 wt% WS to HA. Further increase of WS results in a decrease in strength to 0.67 ± 0.14 MPa. The scaffolds show excellent bioactive and dissolution properties in biological solutions with respect to pure HA scaffold. These properties were strongly dependent on the WS content being optimized at a WS/HA weight ratio equal to 1.

It is concluded that the incorporation of well calculated amount of WS into HA influences the mechanical and biological properties of composite scaffolds. The system is a promising candidate as bone graft materials because of the higher dissolution rate, good bioactivity and improved mechanical properties.

References

[1] J.M. Karp, P.D. Dalton, M.S. Shoichet, Scaffolds for tissue engineering, MRS Bulletin 28 (2003) 301–306.
[2] J.R. Jones, L.L. Hench, Regeneration of trabecular bone using porous ceramics, Current Opinion in Solid State and Materials Science 7 (2003) 301–307.
[3] D.W. Hutmacher, Scaffolds in tissue engineering bone and cartilage, Biomaterials 21 (2000) 2529–2543.
[4] R. Langer, J.P. Vacanti, Tissue engineering, Science 260 (1993) 920–926.
[5] V. Karageorgiou, D. Kaplan, Porosity of 3D biomaterial scaffolds and osteogenesis, Biomaterials 26 (2005) 5474–5491.
[6] E. Charriere, J. Lemaitre, P. Zysset, Hydroxyapatite cement scaffolds with controlled macroporosity: fabrication protocol and mechanical properties, Biomaterials 24 (2003) 809–817.
[7] X. Miao, Y. Hu, J. Liu, A.P. Wong, Porous calcium phosphate ceramics prepared by coating polyurethane foams with calcium phosphate cements, Materials Letters 58 (2004) 397–402.
[8] S.H. Li, J.R. De Wijn, P. Layrolle, K. De Groot, Synthesis of macroporus hydroxyapatite scaffolds for bone tissue engineering, Journal of Biomedical Materials Research 61 (2002) 109–120.
[9] H.R. Ramay, M. Zhang, Preparation of porous hydroxyapatite scaffolds by combination of the gel-casting and polymer sponge methods, Biomaterials 24 (2003) 3293–3302.
[10] S.M. Best, A.E. Porter, E.S. Thian, J. Huan, Bioceramics: past, present and for the future, Journal of the European Ceramic Society 28 (2008) 1319–1327.
[11] S.V. Dorozhkin, Bioceramics of calcium orthophosphates, Biomaterials 31 (2010) 1465–1485.
[12] M. Freyman, I.V. Yannas, L.J. Gibson, Cellular materials as porous scaffolds for tissue engineering, Progress in Materials Science 46 (2001) 273–282.
[13] I. Jun, J. Song, W. Choi, Y. Koh, H. Kim, Porous hydroxyapatite scaffolds coated with bioactive apatite–wollastonite glass-ceramics, Journal of the American Ceramic Society 90 (2007) 2703–2708.
[14] X. Miao, L.P. Tan, L.S. Tan, X. Huang, Porous calcium phosphate ceramics modified with PLGA-bioactive glass, Materials Science and Engineering C 27 (2007) 274–279.
[15] S. Ni, J. Chang, L. Chou, A novel bioactive porous $CaSiO_3$ scaffold for bone tissue engineering, Journal of Biomedical Materials Research A 76 (2006) 196–205.
[16] T. Kokubo, A/W glass-ceramic: processing and properties, in: L.L. Hench, J. Wilson (Eds.), An Introduction to Bioceramics, World Scientific, Singapore, 1993, pp. 75–88.
[17] A. Martin, E. Romero, S.A. Salinas, L. Jesus, V. Garcia, S.R. Payan, F.F. Castillón-Barraza, Mechanical and bioactive behavior of hydroxyapatite–wollastonite sintered composites, International Journal of Applied Ceramic Technology 7 (2010) 164–177.
[18] K. Lin, M. Zhang, W. Zhai, H. Qu, J. Chang, Fabrication and characterization of hydroxyapatite/wollastonite composite bioceramics with controllable properties for hard tissue repair, Journal of the American Ceramic Society 94 (2011) 99–105.
[19] F. Gervaso, F. Scalera, S. Kunjalukkal Padmanabhan, A. Sannino, A. Licciulli, High performance hydroxyapatite scaffolds for bone tissue engineering applications, International Journal of Applied Ceramic Technology 9 (2012) 507–516.
[20] S. Kunjalukkal Padmanabhan, M. Carrozzo, F. Gervaso, F. Scalera, A. Sannino, A. Licciulli, Mechanical performance and in vitro studies of hydroxyapatite/wollastonite scaffold for bone tissue engineering, Key Engineering Materials 855 (2011) 493–494.
[21] K.P. Sanosh, M.C. Chu, A. Balakrishnan, T.N. Kim, S.J. Cho, Preparation and characterization of nano-hydroxyapatite powder using sol–gel technique, Bulletin of Materials Science 32 (2009) 465–470.

[22] T. Kokubo, H. Kushitani, S. Sakka, T. Kitsugi, T. Yamamuro, Solutions able to reproduce in vivo surface-structure changes in bioactive glass ceramic, Journal of Biomedical Materials Research 24 (1990) 721–734.
[23] K.L. Lin, J. Chang, J.X. Lu, J.H. Gao, Y. Zeng, Properties of beta-$Ca_3(PO_4)_2$ bioceramics prepared using nano-size powders, Ceramics International 33 (2007) 979–985.
[24] V. Karageorgiou, D. Kaplan, Porosity of 3D biomaterial scaffolds and osteogenesis, Biomaterials 26 (2005) 5474–5491.
[25] E. Tsuruga, H. Takita, H. Itoh, Y. Wakisaka, Y.Y. Kuboki, Pore size of porous hydroxyapatite as the cell-substratum controls BMP induced osteogenesis, Journal of Biochemistry 121 (1997) 317–324.
[26] W.A. Deer, R.A. Howie, J. Zussman, Wollastonite, Rock Forming Minerals, Longmans, London, 1963.
[27] F.P. Knudsen, Dependence of mechanical strength of brittle polycrystalline specimens on porosity and grain size, Journal of the American Ceramic Society 42 (1959) 376–387.
[28] B.Q. Liu, C.Z. Huang, M.L. Gu, H.T. Zhu, H.L. Liu, Preparation and mechanical properties of in situ growth TiC whiskers toughening Al_2O_3 ceramic matrix composite, Materials Science and Engineering A 146 (2007) 460–461.
[29] C. Wu, Y. Ramaswamy, P. Boughton, H. Zreiqat, Improvement of mechanical and biological properties of porous $CaSiO_3$ scaffolds by poly(D,L-lactic acid) modification, Acta Biomaterialia 4 (2008) 343–353.
[30] Q.Z. Chen, I.D. Thompson, A.R. Boccaccini, 45S5 bioglass-derived glass-ceramic scaffolds for bone tissue engineering, Biomaterials 27 (2006) 2414–2425.
[31] L.J. Gibson, M.F. Ashby, Cellular Solids: Structure and Properties, Pergamon Press, Oxford, 1999, pp. 429–452.
[32] W. Xue, X. Liu, X. Zheng, C. Ding, Dissolution and mineralization of plasma-sprayed wollastonite coatings with different crystallinity, Surface and Coatings Technology 200 (2005) 2420–2427.
[33] L.L. Hench, J.M. Polak, Third-generation biomedical materials, Science 295 (2002) 1014–1017.
[34] L. Radev, V. Hristov, B. Samuneva, D. Ivanova, Organic/inorganic bioactive materials part II: in vitro bioactivity of collagen–calcium phosphate silicate/wollastonite hybrids, Central European Journal of Chemistry 7 (2009) 711–720.
[35] H.S. Ryu, J.K. Lee, H. Kim, K.S. Hong, Materials: hydroxyapatite/a-wollastonite composites, Journal of Materials Research 20 (2005) 1154–1162.